



OPEN

## Evaluation of the nano silica and nano waste materials on the corrosion protection of high strength steel embedded in ultra-high performance concrete

Sahar A. Mostafa<sup>1</sup>, Mohamed M. EL-Deeb<sup>2✉</sup>, Ahmed A. Farghali<sup>3</sup> & A. Serag Faried<sup>4</sup>

Corrosion resistance of high strength steel (HSS) embedded in ultra-high performance concrete (UHPC) immersed in 3.5% NaCl solution is evaluated in the absence and presence of nano silica (NS), nano glass waste (NGW), nano rice husk ash (NRHA) and nano metakaolin (NMK) using open circuit potential, potentiodynamic polarization and electrochemical impedance spectroscopy (EIS) under normal and accelerated conditions. Data showed that the corrosion rate in the accelerated conditions is higher compared by the normal conditions due to the increasing in the rate of both anodic and cathodic reactions in the presence of anodic current. On the other hand, the presence of the studied nano materials decreases both the anodic and cathodic overpotentials, and shifts both the open circuit potential ( $E_{ocp}$ ) and corrosion potential ( $E_{corr}$ ) of HSS to more noble values, as well as decreases the values of the corrosion current densities ( $I_{corr}$ ) in both normal and accelerated conditions. Furthermore, EIS analysis illustrates that the presence of these materials enhances both the concrete bulk resistance and the charge transfer resistance at HSS/UHPC interface, which retards the flow of the electrons between the anodic and cathodic sites, thus impeding the propagation of the corrosion process. The inhibitory effect of the studied nano materials for the corrosion of HSS is interpreted on the basis of the change in the microstructure and the compressive strength of the UHPC.

Concrete is considered as the backbone of the construction industry all over the world from an economic point of view. However, its high brittleness, relatively low tensile-to-compressive strength and insufficient flowability as well as exposure to the aggressive marine environment causes a global concern over its lifespan<sup>1,2</sup>. Therefore, ultra-high performance concrete (UHPC) is considered as a new generation of cementitious composite that has been recently used in the construction infrastructures technology. The advantages of the UHPC compared to ordinary concrete are concerned to its extraordinary properties such as strength, durability, ductility, very low water/binder ratio and its highly resistance to the environmental conditions<sup>3-6</sup>. UHPC has employed several projects all over the world and has gained interests in complicated applications such as architectural features, bridges, roads, rehabilitation, repair and vertical components; such as utilities towers for gas and oil industry applications, windmills towers, hydraulic structures in different countries<sup>7</sup>.

Nano-technology have revealed that, nano-sized particles with high surface area to volume ratio, that provides the potential for tremendous chemical reactivity to achieve the current challenge to get durable concrete with less cement within reasonable cost. Due to the fact that glass waste is not biodegradable, landfills do not offer an ecological solution. A potential solution providing a sustainable, ecological and economic solution are needed. Investigations proved that a particle size less than 75  $\mu\text{m}$  has a pozzolanic reactivity and positive contribution on the micro-structural properties<sup>8</sup>. The pozzolanic nature of rice husk ash due to high silica content makes it a valuable supplementary cementitious material that reduces the land-filling costs, as well as provides a cleaner sustainable environmental solution in saving energy and reducing carbon dioxide generation by cement consumption<sup>9</sup>.

<sup>1</sup>Department of Civil Engineering, Faculty of Engineering, Beni-Suef University, Beni-Suef 62511, Egypt. <sup>2</sup>Applied Electrochemistry Laboratory, Chemistry Department, Faculty of Science, Beni-Suef University, Beni-Suef 62511, Egypt. <sup>3</sup>Materials Science and Nanotechnology Department, Faculty of Postgraduate Studies for Advanced Sciences, Beni-Suef University, Beni-Suef 62511, Egypt. <sup>4</sup>Department of Civil Engineering, Faculty of Engineering, Fayoum University, Fayoum, Egypt. ✉email: eldeebm@yahoo.com

Corrosion of steel reinforcing steel bar (rebar) in concrete is one of the most important and frequent factor in long-term civil infrastructure failures around the world<sup>10</sup>. Chloride-induced corrosion of rebar is considered as a main reason for steel corrosion in civil infrastructure, that be occurred due to attacks of chloride ions from marine and chloride contaminated environments<sup>11,12</sup>. Numerous materials can be used to improve the microstructures of UHPC, that can decrease the permeability and diffusibility of the chemicals inducing chlorides to the rebar<sup>13,14</sup>, other waste materials are used to improve the shielding effect of the concrete to gamma radiation<sup>15</sup>. Maddalena et. al.<sup>16</sup>, synthesized the relative simplicity, speed, comparative low cost of C-S-H to improve the mechanical and microstructure in the construction industry. UHPC with 1% nano metaclay enhanced the corrosion resistance for embedded steel<sup>17</sup>. The presence of nano silica (NS) in UHPC, effectively delayed the initiation of the corrosion of steel bars. LPR and Tafel results ensured that NS increased the polarization resistance of embedded bars and lowered corrosion rate<sup>14</sup>. Accelerated corrosion test has the most efficiency technique to measure the corrosion resistance. Some studies have revealed that great differences exist between accelerated corrosion and natural corrosion on corrosion products, distribution of corrosion penetration and developing of expansive cracks<sup>18–20</sup>. Corrosion resistance of high performance concrete (HPC), ultra-high performance concrete (UHPC) and UHPC incorporating nano silica (UHPC-ns) was evaluated<sup>14</sup>. Results indicated that the time needed for the first crack was 3600 min, 7000 min, and 8800 min for HPC, UHPC and UHPC-ns respectively, indicating that the corrosion resistance of UHPC-ns is higher than that of UHPC and HPC. Corrosion rate of UHPC-ns was the lowest rate 0.1 mm/year when compared to 0.35 mm/year and 0.17 mm/year for HPC and UHPC respectively. Higher polarization due to nano silica ensures the enhancement of corrosion resistance also corrosion potential dropped in all cases with the similarity in case of HPC and UHPC but  $E_{\text{corr}}$  of UHPC-ns dropped from 0.511 V to 0.58 V with significant values due to nano silica effect in improving the concrete microstructure, strength and durability which plays a vital role in lowering the diffusion of chlorides in the concrete specimens<sup>21</sup>. Nano titanium and nano  $\text{CaCO}_3$  in presence of sodium nitrate achieved noticeable improvement in durability, strength, carbonation and corrosion resistance of green concrete<sup>1</sup>. The inclusion of 1% nano metakaolin enhances the mechanical properties and microstructure of UHPC<sup>22,23</sup>. Tawfik et al.<sup>24</sup>, studied the corrosion rate of reinforcing steel in high-performance concrete using nano additives. They found that the corrosion potentials of the rebar were shifted to more positive values, as well as the corrosion current densities were decreased in the presence of the nano additives compared to control sample.

Aim of our research is to evaluate the effect of nano silica and three types of nano waste materials; nano glass waste (NGW), nano rice husk ash (NRHA) and nano metakaolin (NMK) on the corrosion resistance of HSS embedded in UHPC immersed in 3.5% NaCl solution in normal and accelerated conditions using open circuit potential, Potentiodynamic polarization and electrochemical impedance spectroscopy techniques.

## Experimental

**Materials.** Ordinary Portland Cement (type I, 52.5 grade) supplied from Misr Beni Suef company (Beni Suef city, Egypt) according to ASTM C150<sup>25</sup> is used for casting the concrete specimens. Silica fumes is supplied from Sika Egypt Company with specific surface area of  $16.8 \times 10^3 \text{ m}^2/\text{Kg}$  and 2.15 specific gravity, is used as mineral admixture based on the mass of the cement. The aggregate consisted of crushed dolomite from Ataq mountain quarry with a maximum size of 6.3 mm and specific density of 2.65 as a coarse aggregate, while natural sand with fineness modulus of 2.94 mm as a fine aggregate. The selection of the aggregates is in agreements with ASTM C33<sup>26</sup>. Coarse aggregate is used in saturated surface dry conditions, while fine aggregate is washed, dried and used in dry conditions. Additional amount of water equal to absorption of sand is added to the effective water (w/b). Polycarboxylates water reducer (Sika Viscocrete 3425) with density of  $1.08 \text{ t/m}^3$  is used as a superplasticizer with 1.0–1.5% based on the mass of the cement. 35 mm hooked-end steel fibers with aspect ratio of 43.75 and tensile strength of 1100 MPa are used to improve the ductility and increase the energy absorption of the ultra-high performance concrete (UHPC).

Nano silica (NS) and three types of nano waste materials; nano glass waste (NGW), nano rice husk ash (NRHA) and nano metakaolin (NMK) are prepared in nano sized scale, in our laboratory as discussed previously<sup>23,27–29</sup> which schematically represented in Fig. 1, and their chemical composition are tabulated in Table 1, as well as their microstructure is shown in Fig. 2. The mix design for casting the UHPC specimens is based on Maravelaki-Kalaitzaki et al.<sup>30</sup> and are summarized in Table 2.

**HSS rebar.** The studied high strength steel (HSS) is produced according to Egyptian Standards as deformed bars (ES 262/2009 Gr), its chemical composition as provided from the manufacturer is shown in Table 3.

**Sample geometry.** UHPC cylindrical specimens with 100 mm diameter and 200 mm height are casted for the electrochemical tests. HSS rebar with 16 mm diameter and 200 mm height is embedded in UHPC mix at the middle of the cylindrical specimens at a distance of 42 mm from concrete base as schematically represented in Fig. 3.

**Electrochemical measurements.** All the electrochemical measurements are carried out using the Potentiostat / Galvanostat (AUTOLAB PGSTAT 128 N) as previously reported<sup>31</sup>. In short, standard three-electrode cell with HSS rebar working, saturated Ag/AgCl reference and Pt sheet counter electrodes are used, while NOVA 1.11 software is used to records and fits the electrochemical measurements. Potentiodynamic polarization measurements are achieved in the potential range between  $-100$  to  $+100 \text{ mV}$  vs.  $E_{\text{OCP}}$  values at  $25 \pm 2 \text{ }^\circ\text{C}$  with the scan rate of  $1.0 \text{ mV s}^{-1}$ . Electrochemical impedance spectra at the respective  $E_{\text{OCP}}$  values are recorded using AC signals of amplitude 5 mV peak to peak in the frequency range of 10 kHz to 10 MHz.



**Figure 1.** Preparing of nano waste materials.

Items	SiO <sub>2</sub>	Al <sub>2</sub> O <sub>3</sub>	Fe <sub>2</sub> O <sub>3</sub>	CaO	MgO	SO <sub>3</sub>	K <sub>2</sub> O	Na <sub>2</sub> O	Cl	TiO <sub>2</sub>
NS	95.39	0.15	1.11	0.43	0.09	0.05	0.030	1.790	0.71	–
NWG	72.58	0.17	1.11	12.12	2.09	0.19	0.030	11.700	0.01	–
NMK	89.6	0.9	2.0	0.43	2.0	–	4.55	–	–	0.7
NRHA	92	0.23	0.21	1.39	0.36	1.42	2.99	0.2	0.16	–

**Table 1.** Chemical composition of nano materials.

**Impressed voltage test.** The impressed voltage technique is considered as an accelerated technique used to investigate the corrosion resistance of the rebar<sup>32</sup>. The test setup is represented in Fig. 4, and occurred by immersing the specimens in 3.5% NaCl solution. HSS rebar acts as the anode and a cylindrical steel acts as the cathode, while a constant DC potential of 12 V is impressed between the anode and cathode using a DC power supply.

**Microstructure characterization.** The microstructures of the prepared materials are examined using a Transmission Electron Microscope (JEOL JEM 2100, Japan) with an acceleration voltage of 200, SEM-EDX analysis is carried out using JSM-6510LA (JEOL, Tokyo, Japan). Crystallinity and the phase identification are analyzed using X-ray diffractometer (PANalytical Empyrean, Netherlands) using CuK $\alpha$  radiation (wavelength  $\lambda = 1.54045 \text{ \AA}$ ) at an accelerating voltage 40 kV, current 35 mA.

Raman Spectroscopy RS are illuminated with a 532 nm He–Ne. Laser scanning is carried out by using the syncro mode from 0 to 2000  $\text{cm}^{-1}$ . Data are performed with WiRE3.3 software (Renishaw, Illinois). BET surface area, pore volume and pore size distribution are determined using a surface area analyzer (TriStar II 3020, Micromeritics, USA).

**Compressive strength test.** Concrete cube specimens of size 150 mm  $\times$  150 mm  $\times$  150 mm are casted and subjected to compressive strength test as per ASTM C39<sup>33</sup> using a 3000 kN capacity digital compressive testing machine at the age of 28 days.

## Results and discussion

**Open circuit potentials.** Changes in the open circuit potentials ( $E_{\text{OCP}}$ ) values of HSS embedded in UHPC that been immersed for 50 days in 3.5% NaCl solution in the absence and presence of 1% NS, NGW, NRHA and NMK under normal and accelerated conditions at  $25 \pm 2 \text{ }^\circ\text{C}$  are shown in Fig. 5 and Table 4. Data clearly shows

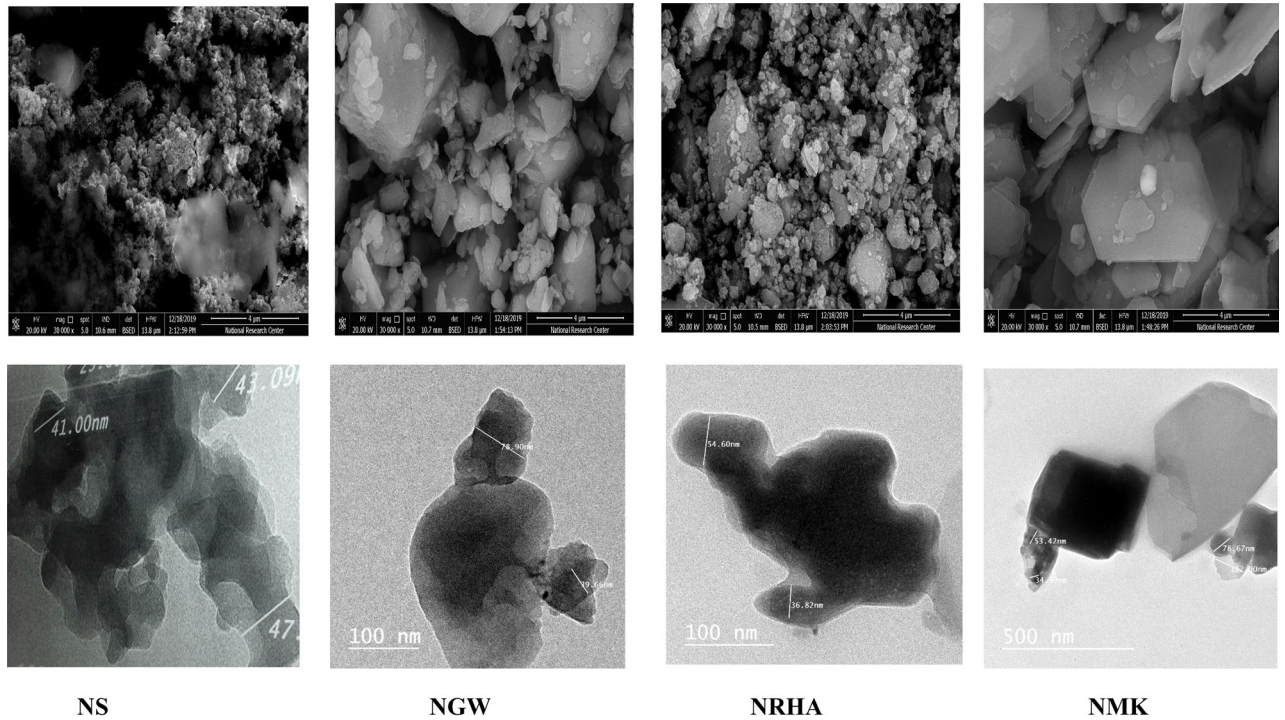


Figure 2. Microstructure of nano silica and nano waste materials.

Sample	Cement (kg/m <sup>3</sup> )	SF (kg/m <sup>3</sup> )	Fine aggregate (kg/m <sup>3</sup> )	Coarse aggregate (kg/m <sup>3</sup> )	Water (kg/m <sup>3</sup> )	SP (kg/m <sup>3</sup> )	Steel fiber % (volume fraction)	NWG %	NS %	NMK %	NRHA %	Compressive strength (MPa)
UHPC	900	135	348.75	776.25	186.3	22.5	1	–	–	–	–	114.7
UHPC-NRHA	900	135	348.75	776.25	186.3	22.5	1	–	–	–	1	118.4
UHPC-NMK	900	135	348.75	776.25	186.3	22.5	1	–	–	1	–	119.8
UHPC-NS	900	135	348.75	776.25	186.3	22.5	1	–	1	–	–	130.9
UHPC-NWG	900	135	348.75	776.25	186.3	22.5	1	1	–	–	–	132.1

Table 2. Mix proportions of UHPC.

Fe	C	Mn	Si	S	P	N	Sn	V	Mo	Cr	Co	CEV
96.948	0.29	1.6	0.55	.040		0.0120	0.56					

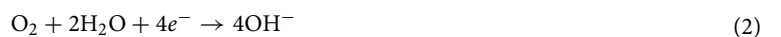
Table 3. Chemical composition of steel rebar.

that, more negative value of Eocp for HSS embedded in the control specimen (UHPC) in accelerating conditions compared by its value in the normal conditions. This results are attributed to the increasing in the rate of both anodic and cathodic reactions in the presence of anodic current, that increases the overall corrosion rate. These reactions can be summarized<sup>11,34</sup> as:

1. The anodic dissolutions of HSS that release electrons and dissolves as ferrous ions as represents in the following equation:



2. These electrons migrate to the cathodic site to reduce O<sub>2</sub> and/or H<sub>2</sub>O as follows:



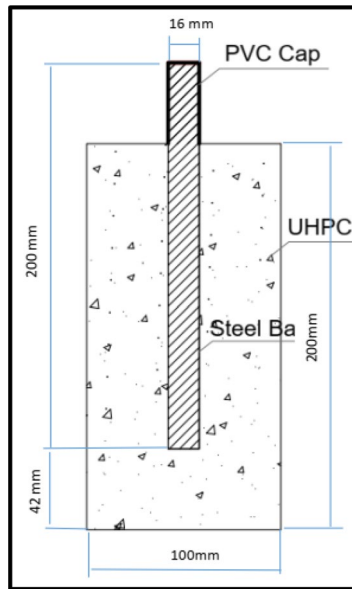


**Figure 3.** Geometry of the HSS rebar (Autocad 2018).

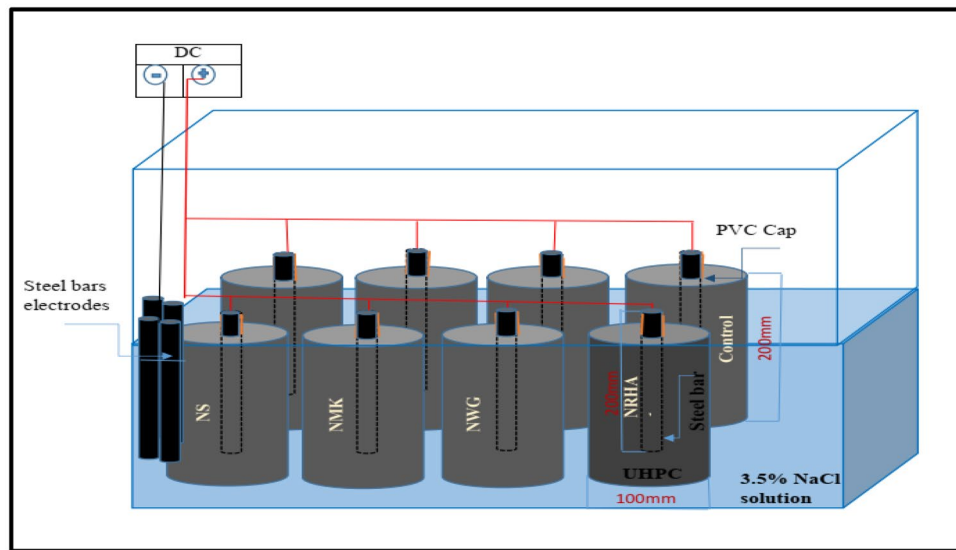


**Figure 4.** Setup for impressed voltage test (Microsoft office 2013).

3. Then  $Fe^{2+}$  contentions to react as follows to form rust:



Also, we can conclude from that figure that, the incorporating of the studied nano materials in UHPC, enhances the corrosion resistance of HSS in both normal and accelerating conditions. This behaviour can be explained as a result of the synergistic effect of these nano materials on the microstructure and mechanical properties of UHPC as summarized in Fig. 6 and Table 2. It is found that, the SEM micrograph of UHPC shows denser microstructure with no evidence of micro cracks propagation in the presence of the studied nano materials

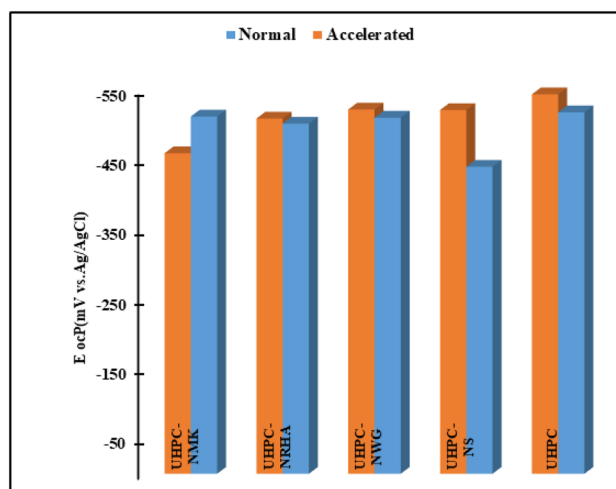


**Figure 5.** variation of  $E_{ocp}$  of HSS embedded in UHPC immersed in 3.5% NaCl in the absence and presence of 1% nano materials at  $25 \pm 2$  °C in both normal and accelerated conditions.

Sample	Accelerated condition					Normal condition				
	$E_{ocp}$ mV (vs. Ag/AgCl)	$E_{corr}$ mV (vs. Ag/AgCl)	$I_{corr}$ ( $\mu\text{A}\cdot\text{cm}^{-2}$ )	$R_p$ ( $\Omega$ )	$C_{Rate}$ mm/year	$E_{ocp}$ mV (vs. Ag/AgCl)	$E_{corr}$ mV (vs. Ag/AgCl)	$I_{corr}$ $\mu\text{A}\cdot\text{cm}^{-2}$	$R_p$ ( $\Omega$ )	$C_{Rate}$ mm/year
UHPC	-544.2	-547.2	39.14	415.8	0.454	-518.3	-520.4	31.72	1060.6	0.369
UHPC-NS	-521.6	-505.8	20.39	808.9	0.237	-440.2	-448.4	07.63	2701.3	0.088
UHPC-NRHA	-509.3	-524.2	16.96	541.6	0.197	-504.1	-513.4	14.49	1682.3	0.168
UHPC-NGW	-522.1	-468.7	12.41	2324.0	0.144	-514.9	-520.9	12.68	1984.3	0.147
UHPC-NMK	-459.9	-522.3	11.92	1217.2	0.138	-512.3	-519.1	25.36	1022.7	0.327

**Table 4.** Electrochemical kinetic parameters of HSS embedded in UHPC immersed in 3.5% NaCl in the absence and presence of 1% nano materials.

compared to UHPC control specimen. Specific surface area of UHPC and its composite with the studied nano materials are studied by BET multi-point method and BJH method. Results of the specific surface area, total pore volume and pore size analysis are tabulated in Table 5. It can be seen from the Table 5 that the incorporation of the nano materials with the UHPC shows microporous structure (pore size < 10 nm) with small both specific surface area and total pore volume, compared to UHPC which follows the following order: UHPC > UHPC-NMK > UHPC-NRHA > UHPC-NGW > UHPC-NS. This observation can be interpreted to the filling effect of these materials on both the pores and the micro cracks of UHPC as well as their effect on the pozzolanic reaction that enhances the compactness structure of the UHPC composite. On the other hand, the order of the dense structure of the UHPC composites are in a good agreement with their measured compressive strength as indicated from Table 2. This improvement in the dense pore structure and the compressive strength of the UHPC composites, enhances the inhibitory effect of the diffusion and penetration of  $\text{O}_2$ ,  $\text{H}_2\text{O}$  and  $\text{Cl}^-$  to HSS/UHPC interface. Therefore, reduces the rate of the cathodic reaction and thereby the overall corrosion rate. On the other hand, the presence of these nano materials increases the electrical resistivity of UHPC that retards the flow of electrons between the anodic and cathodic sites, thus impeding the propagation of the corrosion process<sup>10</sup>. This data is in a good agreement with our EIS measurements.

**Potentiodynamic polarization measurements.** Potentiodynamic polarization measurements are conducted for HSS rebar embedded in UHPC after immersion in 3.5% NaCl solution for 50 days, by changing the electrode potential automatically  $\pm 100$  mV against the  $E_{OCp}$  with scan rate of 1.0 mV/s. Figure 7 represents the anodic and cathodic polarization curves of HSS embedded in UHPC in the absence and presence of 1% NS, NGW, NRHA and NMK, under normal and accelerated conditions at  $25 \pm 2$  °C, while there electro-chemical kinetic parameters are tabulated in Table 4. The results imply that the presence of uniform corrosion without any sign for pitting corrosion within the studied polarization range for all specimens under normal and accelerated conditions. Moreover, the corrosion potential ( $E_{corr}$ ) of the control specimens (UHPC) is found to be -547.2 and -520.4 mV (vs. Ag/AgCl) while the corrosion current density ( $I_{corr}$ ) of 39.14 and 31.72  $\mu\text{A}\cdot\text{cm}^{-2}$  in the accelerated and normal conditions respectively. On the other hand, the calculated corrosion rate ( $C_{Rate}$ ) for HSS in normal condition is 0.369 mm/year compared to 0.454 mm/year in case of accelerated condition. The higher both  $I_{corr}$  and  $C_{Rate}$  with more negative shift in the  $E_{corr}$  for HSS in accelerated condition, compared to normal condition can be attributed to the higher both anodic and cathodic reactions in the presence of anodic current as discussed before.

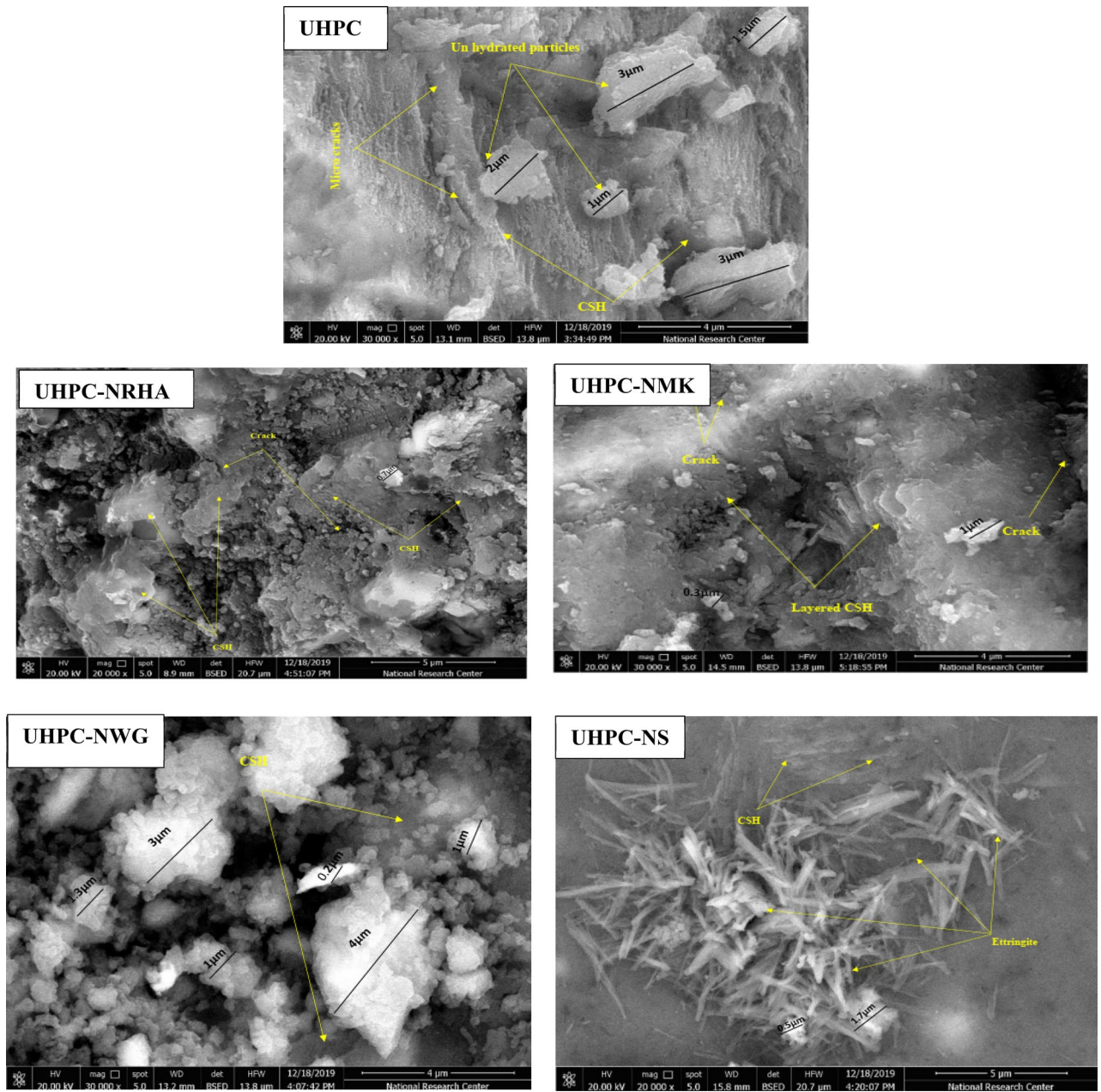


**Figure 6.** SEM micrographs of UHPC in the absence and presence of the studied nano materials.

Samples	S <sub>BET</sub> (m <sup>2</sup> /g)	Total pore volume (cc/g)	Pore size (nm)
UHPC	168.9	0.32	3.8
UHPC-NMK	140	0.75	1.07
UHPC-NRHA	17.46	0.045	4.6
UHPC-NGW	15.2	0.042	5.5
UHPC-NS	7.3	0.037	1.02

**Table 5.** Surface area analysis of UHPC nano composites.

Addition of 1% nano materials to the UHPC, decreases both the anodic and cathodic polarization of HSS, and shifts its E<sub>Corr</sub> to more noble values, as well as decreases both I<sub>Corr</sub> and C<sub>Rate</sub> compared to control specimen in both conditions. Figure 8 shows the variation of I<sub>corr</sub> of HSS as a function in the nano material types, as indicated from the figure, the values of I<sub>corr</sub> are declining from 39.14 μA.cm<sup>-2</sup> for UHPC control specimen in the accelerated conditions to 20.39, 16.69, 12.41 and 11.92 μA.cm<sup>-2</sup> for UHPC-NRHA, UHPC-NS, UHPC-NMK and

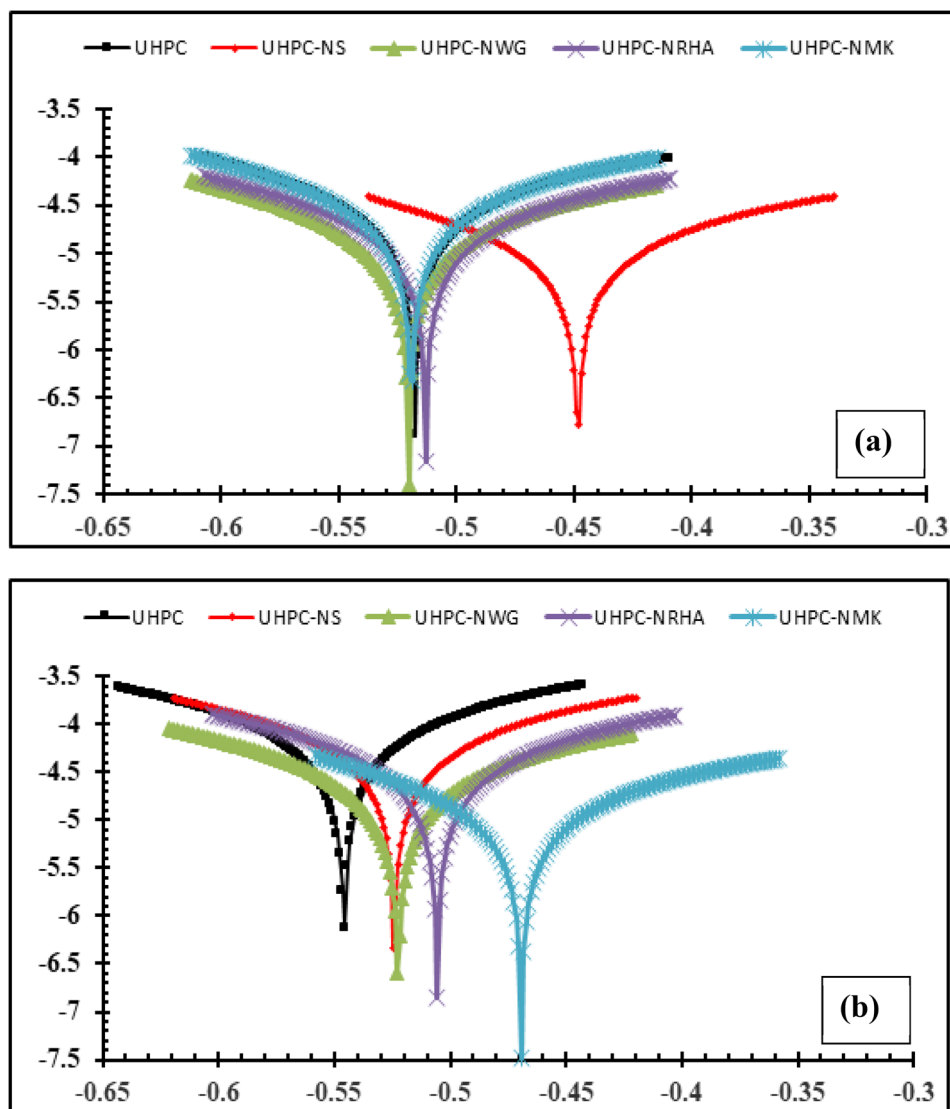


**Figure 7.** Potentiodynamic polarization plots of HSS embedded in UHPC immersed in 3.5% NaCl in the absence and presence of 1% nano materials at  $25 \pm 2^\circ\text{C}$ , with scan rate of 1.0 mV/s in (a) normal and, (b) accelerated conditions.

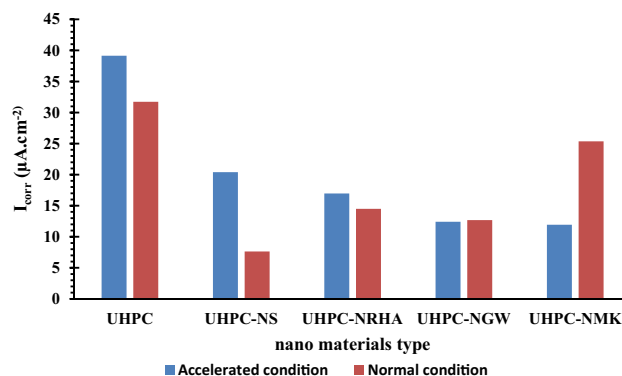


**Figure 8.** Variation of  $I_{\text{corr}}$  of HSS embedded in UHPC immersed in 3.5% NaCl in the absence and presence of 1% nano materials at  $25 \pm 2^\circ\text{C}$  in both normal and accelerated conditions.



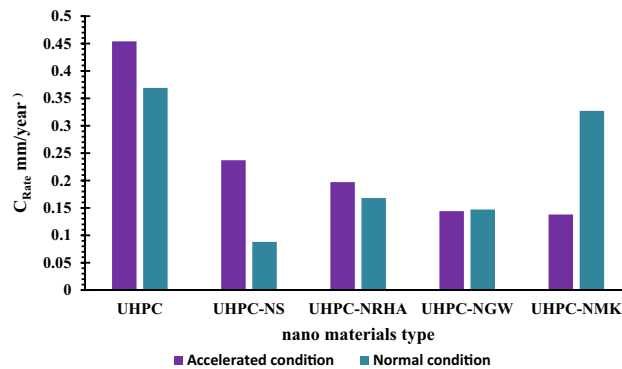


**Figure 9.** Variation of  $C_{Rate}$  of HSS embedded in UHPC immersed in 3.5% NaCl in the absence and presence of 1% nano materials at  $25 \pm 2$  °C in both normal and accelerated conditions.

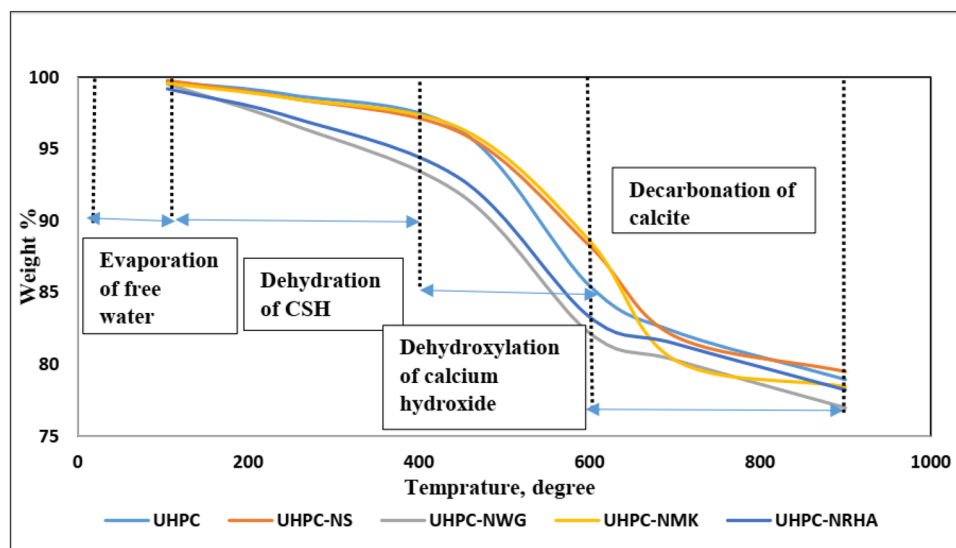


**Figure 10.** TGA thermograms of UHPC in the absence and presence of the studied nano materials.

UHPC-NGW respectively. Also, in the normal condition the values of  $I_{Corr}$  are decreased follows the following order: UHPC > UHPC-NMK > UHPC-NRHA > UHPC-NGW > UHPC-NS. We can conclude from the above results, the incorporating of the studied nano materials during the UHPC mix, increases the corrosion resistance of HSS rebar embedded in UHPC. These results are in a good agreement with the values of the calculated corrosion rate that graphically represented in Fig. 9. This effect is explained on the basis of the dual effect of these nanomaterials which, (1) Effectively filling the micro pores that reduces the permeability and improves the UHPC' microstructure and thus its corrosion resistance as discussed before. (2) Accelerates the rate of the hydration reaction which, acts as the nucleation sites for the formation of the hydration products; calcium hydroxide (CH) and calcium silicate hydrate (CSH). On the other hand, the presence of active  $SiO_2$  in these nano materials, enhances the CSH/CH ratio, which increases the gel pore in UHPC microstructure, that leads to improving its mechanical properties; as observed in its compressive strength (c.f. Table 2), and thereby its corrosion resistance. Figure 10 shows TGA thermograms of UHPC in the absence and presence of the studied nano materials, while the variation of CH and CSH %, that been calculated from TGA data based on Taylor's equation<sup>35</sup>, are graphically represented in Fig. 11. Results show that the CSH% increases with the following order: UHPC < UHPC-NRHA < UHPC-NMK < UHPC-NS < UHPC-NGW. This order is well agreement with our results of the values of both HSS corrosion resistance and UHPC compressive strength. Also, XRD results clarify the presence of diffraction peaks corresponds to CSH at  $2\theta$  values of 26.8°, 33.1°, 40.9°, 58.8°, 70.8° and 81.3° (JCPDS 00-029-0373)<sup>1</sup> with high intensity in the UHPC incorporating with nano materials compared to UHPC control specimen as shown in Fig. 12. This can be interpreted to the increasing in the rate of the hydration reaction and thereby the hydration products, as a result of the incorporation of the nano materials to UHPC. This finding is agreed well with the higher Ca/Si molar ratio which is calculated using EDX analysis in the presence of the studied nano materials as shown in Fig. 13. Moreover, Fig. 14 shows Raman patterns for UHPC and its composites with nano materials to assign the characteristic Raman shifts, as a reference to identify each individual components in the hydration process. It is observed that the characteristic peak of silica fume is observed as a strong and unique at  $517\text{ cm}^{-1}$ ,

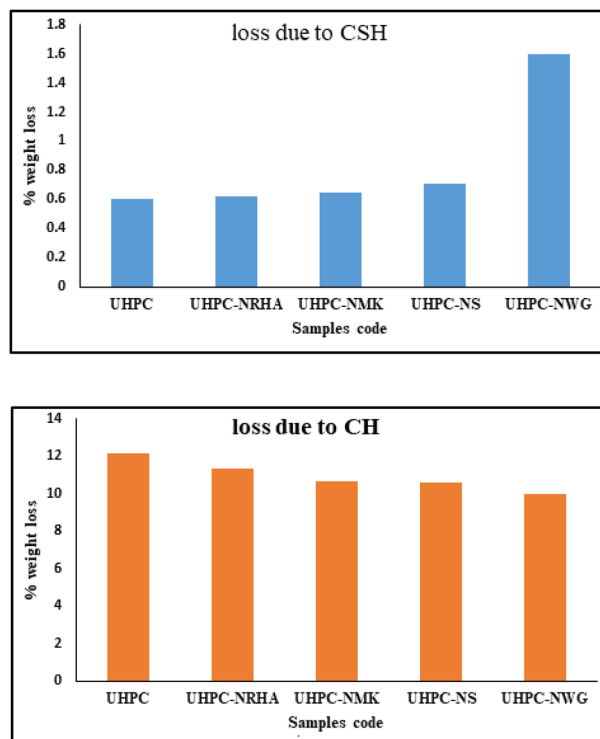


**Figure 11.** Variation of CSH & CH % as a function of the studied nano materials.

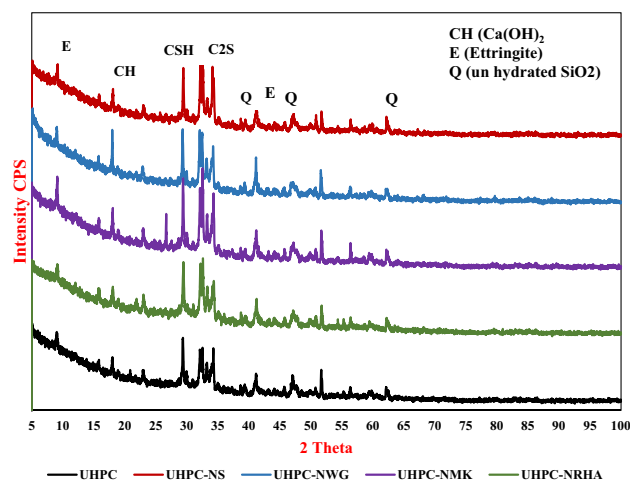


**Figure 12.** XRD spectra the studied nano materials composites.

with different intensity due to pozzolanic reactivity and silica reinforced nano materials. Its highest intensity is obtained at UHPC-NS composite, due to the overlapping between nano silica and silica fume. In addition, silica fume can react with calcium hydroxide (CH) in the presence of water during hydration process, resulting calcium silicate hydrate (CSH) which observed as strong and highest intensity at  $342$  and  $665.58\text{--}711.4\text{ cm}^{-1}$  for UHPC, at  $339.7$  and  $638\text{--}684.51\text{ cm}^{-1}$  for UHPC-NS, at  $340.3$  and  $647\text{--}671\text{ cm}^{-1}$  for UHPC-NMK, at  $337.4$  and  $647.2\text{--}671\text{ cm}^{-1}$  for UHPC-NWG and at  $337$  and

$641.8\text{--}709\text{ cm}^{-1}$  for UHPC-NRHA. Also, calcium hydroxide (CS) peaks decreased in the presence of nano materials, that can be explained to the effect of these nano materials on the rate of the pozzolanic reaction<sup>36</sup>. Also, the highly pozzolanic reaction and phase transfer in UHPC nanocomposites compared to UHPC is observed from the higher CSH/CH phase ratio in case of nanocomposites. This finding is in a good agreement with the previous results which is calculated from the TGA thermograms.

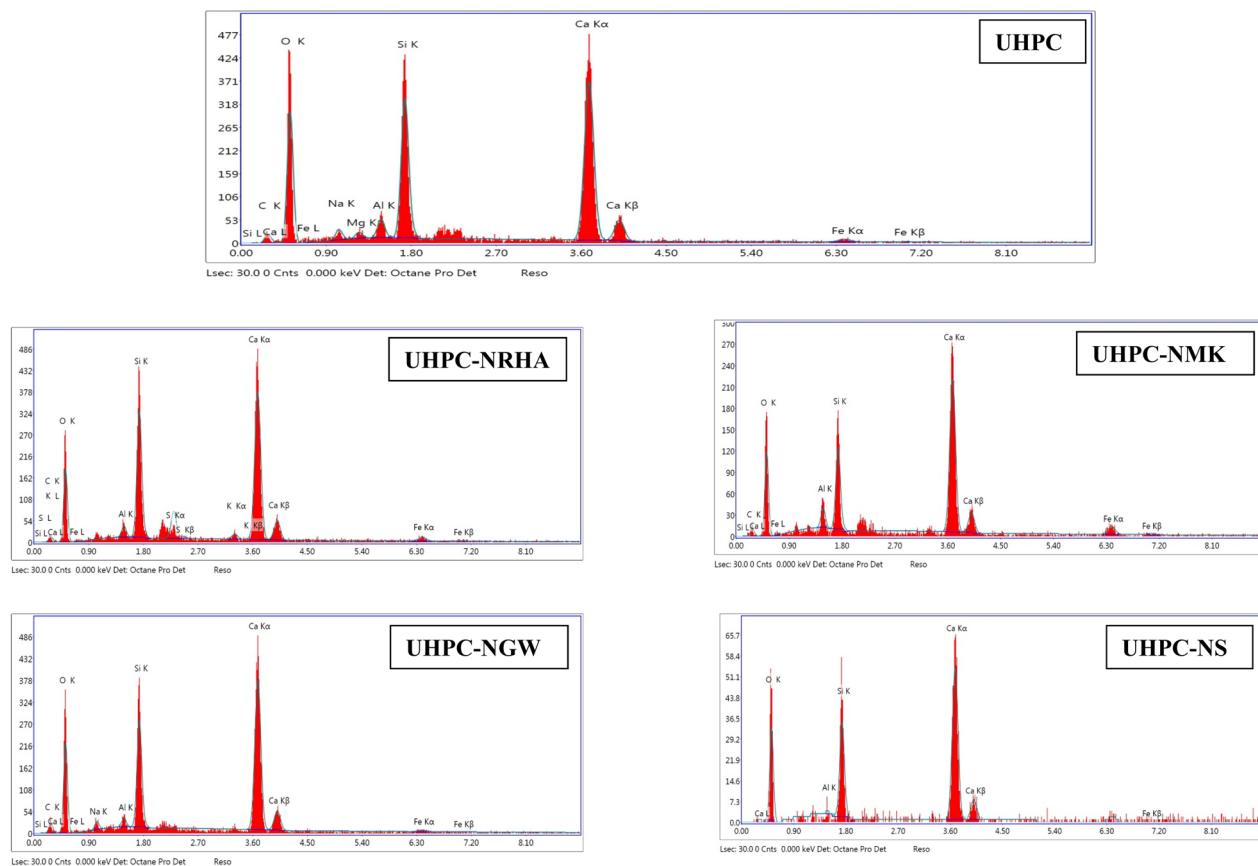


**Figure 13.** EDX analysis of UHPC in the absence and presence of the studied nano materials.

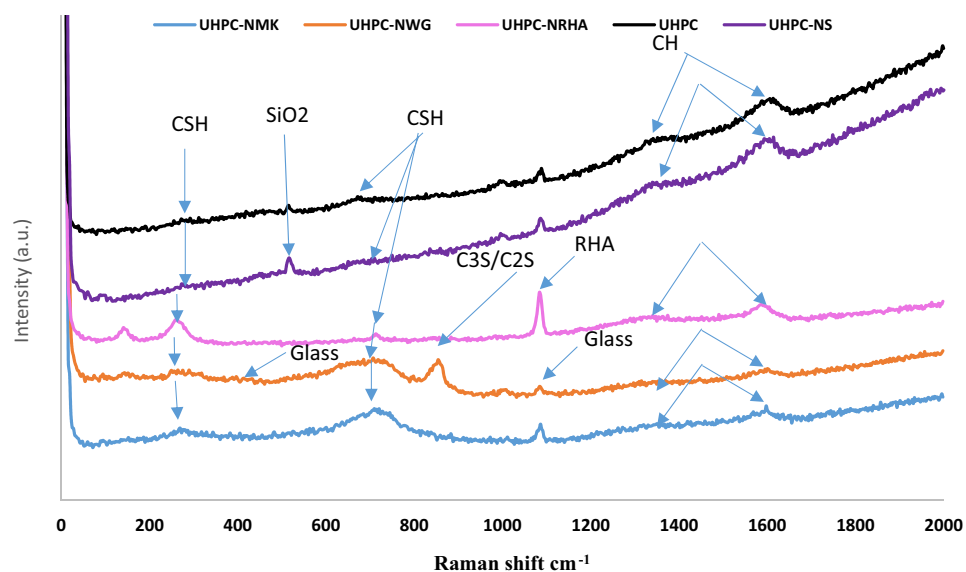


**Figure 14.** Raman spectroscopy for UHPC in the absence and presence of nano materials.

**Electrochemical impedance spectroscopy.** EIS is a non-destructive useful technique which provides a detailed characteristic about Metal/solution and Metal/concrete interface<sup>37–39</sup>. Figure 15 represents the Nyquist plots of HSS embedded in UHPC in the absence and presence of NS, NWG, NRHS and NMK in both normal and accelerated conditions at Eocp over the frequency range of 100 kHz to 10 MHz. Data point out that the presence of two consecutive capacitive semicircles, that have been interpreted to the dielectric properties of the concrete bulk in the high frequency region and to the steel/concrete interface at low frequency region<sup>40</sup>. The

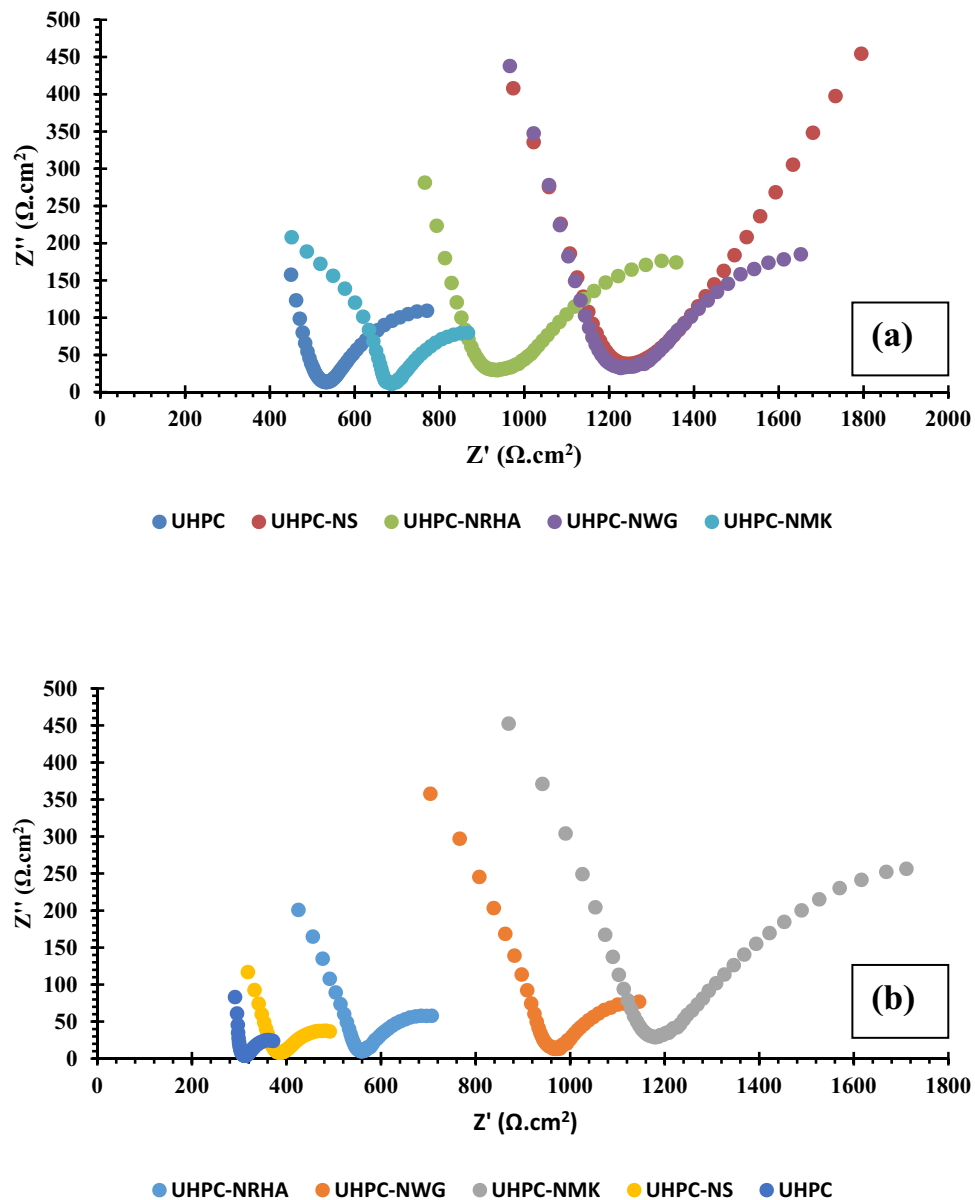


**Figure 15.** Nyquist plots of HSS embedded in UHPC immersed in 3.5% NaCl in the absence and presence of 1% nano materials at  $25 \pm 2$  °C at  $E_{OCP}$  in (a) normal and, (b) accelerated conditions.

diameter of these capacitive loops increases without any change in the shapes of the Nyquist plots in the presence of the studied nano materials, suggesting the mechanism of the corrosion resistance in the absence and presence of these materials is not changed<sup>39</sup>. The increase in the diameters of both two capacitive loops that equivalent to the concrete resistance and charge transfer resistance can be explained to the effect of these materials on the microstructure of the UHPC as discussed before. Denser microstructure due to the effective filling of pore by these nano materials, retards the diffusion of the corrosive ions and  $H_2O/O_2$  molecules through the UHPC bulk to the HSS/UHPC interface. Therefore, decreases both the anodic dissolution of HSS and the cathodic reduction of  $O_2$  and/or  $H_2O$ . This finding indicates the corrosion resistance has been enhanced and the increase in the capacitive loops diameter follows the following order: UHPC < UHPC-NMK ~ UHPC-NRHA < UHPC-NWG ~ UHPC-NS in the normal conditions and in the accelerated conditions as per: UHPC < UHPC-NS < UHPC-NRHA < UHPC-NWG < UHPC-NMK.

Figure 16 illustrates the Bode plots obtained for HSS embedded in UHPC, data shows a broad time constant joined by two time constants at high and low frequency regions that attributed to dielectric properties for the concrete and the HSS/UHPC interface as discussed before. The conjunction of the two time constants indicating that the frequency responses of the two time constants are similar<sup>41</sup>. On the other hand, gradual increase of both the area under the curve and phase angle in the presence of these materials compared to the control specimen

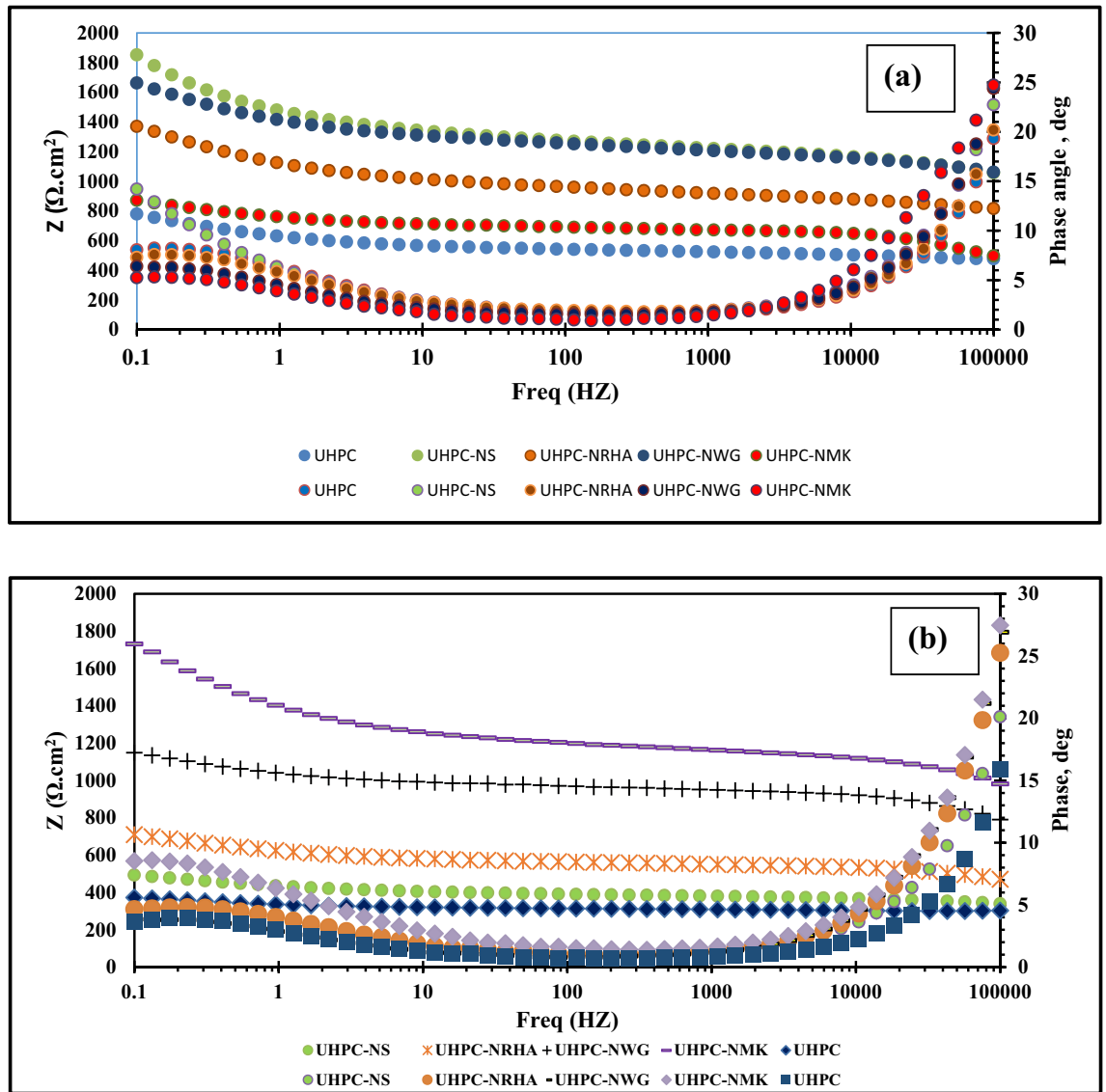


**Figure 16.** Bode plots of HSS embedded in UHPC immersed in 3.5% NaCl in the absence and presence of 1% nano materials at  $25 \pm 2$  °C at  $E_{\text{OCP}}$  in (a) normal and, (b) accelerated conditions.

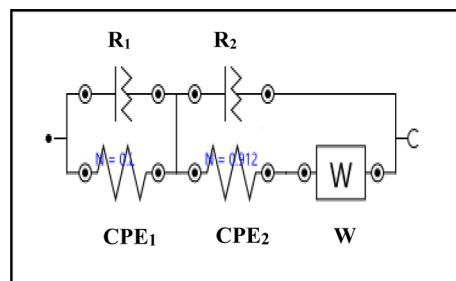


**Figure 17.** Fitted electrochemical equivalent circuit model using NOVA 1.11 software.

means the improvement of the UHPC' resistance against the diffusion of the corrosive ions, and thus increases the corrosion resistance for the HSS<sup>42–44</sup>.

The experimental data are fitted to an electrochemical equivalent circuit based on the Boukamp model<sup>45</sup>, and its model is represented in Fig. 17. It can be seen that the Nyquist plots show  $[RQ/Q(RW)]$  equivalent circuit with two-time constant that agreed with the electrochemical equivalent circuit that fitted steel/ concrete systems<sup>11,46–50</sup>. In this model,  $R_1$  and  $R_2$  denote the concrete and charge transfer resistances respectively, while the

dielectric properties of the concrete bulk and HSS/UHPC interface are represented by  $CPE_1$  and  $CPE_2$ . Moreover, the diffusion of the charged species is represented by Warburg impedance ( $W$ )<sup>11</sup>. The replacement of pure double layer capacitance ( $C_{dl}$ ) with both constant phase element (CPE) and phase shift (N) aims to the compensation of the depression of semicircles in the Nyquist plots that related to the surface roughness. The calculated values of  $R_2$  and  $CPE_2$  of HSS embedded in UHPC corresponding to the charge transfer reaction through the corrosion process shows a change in the structure of the HSS/UHPC interface in both normal and accelerating conditions for nano composite samples compared to UHPC. Data clarify that, increasing the values of the charge transfer resistance ( $R_2$ ) and decreasing the values of the constant phase elements ( $CPE_2$ ) are observed in the presence of nano materials as per the following order: UHPC ( $R_2 = 502 \Omega$ ,  $CPE_2 = 3.7 \times 10^3 \mu Mho$ ), UHPC-NMK ( $R_2 = 750 \Omega$ ,  $CPE_2 = 3.4 \times 10^3 \mu Mho$ ), UHPC-NRHA ( $R_2 = 866 \Omega$ ,  $CPE_2 = 3.1 \times 10^3 \mu Mho$ ), UHPC-NWG ( $R_2 = 1.25 k\Omega$ ,  $CPE_2 = 1.75 \times 10^3 \mu Mho$ ), UHPC-NS ( $R_2 = 2.33 k\Omega$ ,  $CPE_2 = 0.8 \times 10^3 \mu Mho$ ) in the normal conditions and in the accelerated conditions as follows: UHPC ( $R_2 = 231 \Omega$ ,  $CPE_2 = 4.1 \times 10^3 \mu Mho$ ), UHPC-NS ( $R_2 = 362 \Omega$ ,  $CPE_2 = 3.4 \times 10^3 \mu Mho$ ), UHPC-NRHA ( $R_2 = 399 \Omega$ ,  $CPE_2 = 2.9 \times 10^3 \mu Mho$ ), UHPC-NGW ( $R_2 = 1.68 k\Omega$ ,  $CPE_2 = 2.1 \times 10^3 \mu Mho$ ), UHPC-NMK ( $R_2 = 2.23 k\Omega$ ,  $CPE_2 = 0.7 \times 10^3 \mu Mho$ ). This behaviour can be explained to the effect of the studied nano materials on the UHPC microstructure which retards both the diffusion and the penetration rates of  $H_2O$  molecules with high dielectric constant to HSS/UHPC interface. Therefore, the charge transfer reaction is decreased and consequently the corrosion protection is enhanced.

## Conclusion

1. Corrosion resistance of HSS embedded in UHPC immersed in 3.5% NaCl in the absence and presence of 1% NS, NWG, NMK and NRHA is evaluated using open circuit potential, potentiodynamic polarization and electrochemical impedance spectroscopy techniques under normal and accelerated conditions.
2. Incorporation of the studied nano materials in UHPC, shifts both the  $E_{ocp}$  and  $E_{corr}$  of HSS to more noble values without any sign for the pitting corrosion, as well as decreases its  $I_{corr}$  compared to the control specimen in the normal and accelerated conditions.
3. EIS analysis illustrates that the presence of the studied nano materials enhances both the concrete bulk resistance and the charge transfer resistance at HSS/UHPC interface.
4. TGA analysis showed the order of the weight loss due to the dehydration of CSH is agreed with the order of the compressive strength and the corrosion resistance.
5. The inhibitory effect of the studied nano materials for the corrosion of HSS is interpreted on the basis of the change in the microstructure of UHPC that retards both the (1) diffusion of the corrosive ions and/or  $H_2O/O_2$  molecules through the UHPC bulk to the HSS/UHPC interface, and (2) the flow of the electrons between the anodic and cathodic sites, thus impeding the propagation of the corrosion process.

Received: 27 August 2020; Accepted: 19 January 2021

Published online: 28 January 2021

## References

1. Harilal, M. *et al.* High performance green concrete (HPGC) with improved strength and chloride ion penetration resistance by synergistic action of fly ash, nanoparticles and corrosion inhibitor. *Constr. Build. Mater.* **198**, 299 (2019).
2. Yoo, D. Y., Gim, J. Y., & Chun, B. Effects of rust layer and corrosion degree on the pullout behavior of steel fibers from ultra-high-performance concrete. *J. Mater. Res. Technol.* **9**, 3632 (2020).
3. Fan, L., Meng, W., Teng, L. & Khayat, K. H. Effects of lightweight sand and steel fiber contents on the corrosion performance of steel rebar embedded in UHPC. *Constr. Build. Mater.* **238**, 117709 (2020).
4. Meng, W., Khayat, K. H. & Bao, Y. Flexural behaviors of fiber-reinforced polymer fabric reinforced ultra-high-performance concrete panels. *Cem. Concr. Compos.* **93**, 43 (2018).
5. Meng, W. & Khayat, K. H. Improving flexural performance of ultra-high performance concrete by rheology control of suspending mortar. *Compos. B Eng.* **117**, 26 (2017).
6. Schmidt, M. & Fehling, E. Ultra-high-performance concrete: research, development and application in Europe. *ACI Spec. Publ.* **228**, 51 (2005).
7. Azmee, N. M. & Shafiq, N. Ultra-high performance concrete: from fundamental to applications. *Case Stud. Constr. Mater.* **9**, e00197 (2018).
8. Aly, M., Hashmi, M. S. J., Olabi, A. G., Messeiry, M. & Hussain, A. I. Effect of nano clay particles on mechanical, thermal and physical behaviours of waste-glass cement mortars. *Mater. Sci. Eng. A* **528**, 7991–7998 (2011).
9. Kaur, R., Sandhu, R., & Siddique, R. Influence of rice husk ash (RHA) on the properties of self-compacting concrete: a review. *Construct. Build. Mater.* **153**, 751–764 (2017).
10. Abosrra, L., Ashour, A. F. & Youseffi, M. Corrosion of steel reinforcement in concrete of different compressive strengths. *Constr. Build. Mater.* **25**, 3915 (2011).
11. Lu, Y., Hu, J., Li, S. & Tang, W. Active and passive protection of steel reinforcement in concrete column using carbon fiber reinforced polymer against corrosion. *Electrochim. Acta* **278**, 124 (2018).
12. Koleva, D. A. *et al.* Quantitative characterization of steel/cement paste interface microstructure and corrosion phenomena in mortars suffering from chloride attack. *Corros. Sci.* **48**, 4001 (2006).
13. Meng, W. & Khayat, K. H. Mechanical properties of ultra-high-performance concrete enhanced with graphite nanoplatelets and carbon nanofibers. *Compos. B Eng.* **107**, 113 (2016).
14. Ghafari, E., Arezoumandi, M., Costa, H. & Julio, E. Influence of nano-silica addition on durability of UHPC. *Constr. Build. Mater.* **94**, 181 (2015).
15. Baalamurugan, J., Ganesh Kumara, V., Chandrasekaran, S., Balasundar, S., Venkatraman, B., Padmapriya, R., & Bupesh Raja, V. K. Utilization of induction furnace steel slag in concrete as coarse aggregate for gamma radiation shielding. *J. Hazard. Mater.* **369**, 561–568 (2019).
16. Maddalena, R., Li, K., Chater, P. A., Michalik, S. & Hamilton, A. Direct synthesis of a solid calcium-silicate-hydrate (C-S-H). *Constr. Build. Mater.* **223**, 554–565 (2019).

17. Md Jaafar, M. F., Mohd Saman, H., Ariffin, N. F., Muthusamy, K., Ahmad, S. W., & Ismail, R. Corrosion monitoring on steel reinforced nano metaclayed UHPC towards strain modulation using fiber Bragg grating sensor. *Mater. Sci. Eng.* **431**, 122006 (2018).
18. Wang, X., Song, X., Zhang, M. & Du, X. Experimental comparison of corrosion unevenness and expansive cracking between accelerated corrosion methods used in laboratory research. *Constr. Build. Mater.* **153**, 36 (2017).
19. Zhang, W. P., Wang, X. G., Gu, X. L. & Shang, D. F. Comparative study on structural performance of reinforced concrete beams subjected to natural corrosion and accelerated corrosion. *J. Southeast Univ.* **36**, 139 (2006).
20. Yuan, Y. S., Ji, Y. S. & Shah, S. P. Comparison of two accelerated corrosion techniques for concrete structures. *ACI Struct. J.* **104**(3), 344–347 (2007).
21. Yu, R., Spiesz, P., & Brouwers, H. J. H. Effect of nano-silica on the hydration and microstructure development of ultra-high performance concrete (UHPC) with a low binder amount. *Constr. Build. Mater.*, **65**, 40–150 (2014).
22. Muhd Norhasri, M. S., Hamidah, M. S., Mohd Fadzil, A., & Megawati, O. Inclusion of nano metakaolin as additive in ultra high performance concrete (UHPC). *Constr. Build. Mater.* **127** 167 (2016).
23. Norhasri, M. S. M., Hamidah, M. S. & Fadzil, A. M. Inclusion of nano metaclayed as additive in ultra-high performance concrete (UHPC). *Constr. Build. Mater.* **201**, 590 (2019).
24. Tawfik, T., El-Yamani, M., Abde El-Aleem, S., Gabr, A., & Abd El-Hafez, Gh. Effect of nano-silica and nano-waste material on durability and corrosion rate of steel reinforcement embedded in high-performance concrete. *Asian J. Civ. Eng.* **20**, 135 (2019).
25. ASTM C150/C150M-18, Standard Specification for Portland Cement, (ASTM International, West Conshohocken, PA, 2018).
26. ASTM C33, C33M-16e1, Standard Specification for Concrete Aggregates (ASTM International, West Conshohocken, PA, 2016).
27. El-Didamony, H., El-Fadaly, E., Amer, A. A. & Abazeed, I. H. Synthesis and characterization of low cost nanosilica from sodium silicate solution and their applications in ceramic engobes. *Bol. Soc. Esp. Cerám. Vidr* **59**, 31 (2020).
28. Vieira, A. P., Toledo, R. D., Filho Tavares, L. M., & Cordeiro, G. C. Effect of particle size, porous structure and content of rice husk ash on the hydration process and compressive strength evolution of concrete. *Constr. Build. Mater.* **236**, 117553 (2020).
29. Praveenkumar, T. R. & Vijayalakshmi, M. M. Microstructural properties of nano-rice husk ash concrete. *Nanotechnol. Environ. Eng.* **4**, 9 (2019).
30. Maravelaki-Kalaitzaki, P., Agioutantis, Z., Lionakis, E., Stavroulaki, M. & Perdikatsis, V. Physico-chemical and mechanical characterization of hydraulic mortars containing nano-titania for restoration applications. *Cement. Concrete Comp.* **36**, 33 (2013).
31. EL-Deeb, M. M. Role of S<sup>2-</sup> ions on the microstructure change and the pitting behaviour of aluminum in saline solution. *Sci. Rep.* **9**, 11978 (2019).
32. Ha, T. H. *et al.* accelerated short-term techniques to evaluate the corrosion performance of steel in fly ash blended concrete. *Build. Environ.* **42**, 78 (2007).
33. ASTM C39/C39M-18, *Standard Test Method for Compressive Strength of Cylindrical Concrete Specimens* (ASTM International, West Conshohocken, PA, 2017).
34. Chen, J., Fu, C., Ye, H. & Jin, X. Corrosion of steel embedded in mortar and concrete under different electrolytic accelerated corrosion methods. *Constr. Build. Mater.* **241**, 117971 (2020).
35. Jain, J. & Neithalath, N. Analysis of calcium leaching behavior of plain and modified cement pastes in pure water. *Cem. Concr. Compos.* **31**, 176 (2009).
36. Hasanzadeh, B., Liu, F. & Sun, Z. Monitoring hydration of UHPC and conventional paste by quantitative analysis on Raman patterns. *Constr. Build. Mater.* **114**, 208 (2016).
37. Hu, J., Koleva, D. A., deWit, J. H. W., Kolev, H., & Breugel, K. V. Corrosion performance of carbon steel in simulated pore solution in the presence of micelles. *J. Electrochem. Soc.* **158**, 76 (2011).
38. Xu, J. & Yao, W. Electrochemical studies on the performance of conductive overlay material in cathodic protection of reinforced concrete. *Constr. Build. Mater.* **25**, 2655 (2011).
39. EL-Deeb, M. M., Alshammari, H. M., & Abdel-Azeim, S. Effect of ortho-substituted aniline on the corrosion protection of aluminium in 2 mol/L H<sub>2</sub>SO<sub>4</sub> solution. *Can. J. Chem.* **95** 612 (2017).
40. Vedalakshmi, R. & Palaniswamy, N. Analysis of the electrochemical phenomenon at the rebar-concrete interface using the electrochemical impedance spectroscopic technique. *Mag. Concrete Res.* **62**, 177 (2010).
41. Pech-Canul, M. A. & Castro, P. Corrosion measurements of steel reinforcement in concrete exposed to a tropical marine atmosphere. *Cem. Concr. Res.* **32**, 491 (2002).
42. Guan, F. *et al.* Influence of sulfate-reducing bacteria on the corrosion behaviour of 5052 aluminum alloy. *Surf. Coat. Tech.* **316**, 171 (2017).
43. Fan, L., Tang, F., Chen, G., Reis, S. T. & Koenigstein, M. Corrosion resistance of steel pipe coated with two types of enamel by two coating processes. *J. Mater. Eng. Perform.* **27**, 5341 (2018).
44. Fan, L., Reis, S. T., Chen, G., Koenigstein, M. Impedance models and water transport behaviour of steel pipe coated with cathodically polarized enamel. National Association of corrosion Engineers (NACE). International Corrosion 2018, Phoenix, Arizona (2018).
45. Boukamp, B. A. A nonlinear least squares fit procedure for analysis of immittance data of electrochemical systems. *Solid State Ionics* **20**, 31 (1986).
46. Xu, J. X., Jiang, L. H. & Wang, J. X. Influence of detection methods on chloride threshold value for the corrosion of steel reinforcement. *Constr. Build. Mater.* **23**, 1902 (2009).
47. Qiao, G. F. & Ou, J. P. Corrosion monitoring of reinforcing steel in cement mortar by EIS and ENA. *Electrochim. Acta* **52**, 8008 (2007).
48. Montemor, M. F., Simões, A. M. P., & Salta, M. M. Effect of fly ash on concrete reinforcement corrosion studied by EIS. *Cement Concr. Comp.* **22**, 175 (2000).
49. Christodoulou, C., Goodier, C. I., Austin, S. A., Webb, J. & Glass, G. On-site transient analysis for the corrosion assessment of reinforced concrete. *Corros. Sci.* **62**, 176 (2012).
50. Monticelli, C. *et al.* A study on the corrosion of reinforcing bars in alkali-activated fly ash mortars under wet and dry exposures to chloride solutions. *Cem. Concr. Res.* **87**, 53 (2016).

### Author contributions

M. M. EL-Deeb, A. Serag Faried and A. A. Farghali planned the work, proposed the basic idea and supervised the work. S. A. Mostafa implemented the experimental work. M. M. EL-Deeb and A. Serag Faried wrote the paper. All authors reviewed the manuscript

### Competing interests

The authors declare no competing interests.

### Additional information

**Correspondence** and requests for materials should be addressed to M.M.E.-D.

**Reprints and permissions information** is available at [www.nature.com/reprints](http://www.nature.com/reprints).

**Publisher's note** Springer Nature remains neutral with regard to jurisdictional claims in published maps and institutional affiliations.



**Open Access** This article is licensed under a Creative Commons Attribution 4.0 International License, which permits use, sharing, adaptation, distribution and reproduction in any medium or format, as long as you give appropriate credit to the original author(s) and the source, provide a link to the Creative Commons licence, and indicate if changes were made. The images or other third party material in this article are included in the article's Creative Commons licence, unless indicated otherwise in a credit line to the material. If material is not included in the article's Creative Commons licence and your intended use is not permitted by statutory regulation or exceeds the permitted use, you will need to obtain permission directly from the copyright holder. To view a copy of this licence, visit <http://creativecommons.org/licenses/by/4.0/>.

© The Author(s) 2021